Magnetic anisotropies and exchange coupling in ultrathin fcc Co(001) structures

B. Heinrich, J. F. Cochran, M. Kowalewski, J. Kirschner,* Z. Celinski, A. S. Arrott, and K. Myrtle
Surface Physics Laboratory, Physics Department, Simon Fraser University, Burnaby, British Columbia, Canada V5A 1S6
(Received 3 June 1991)

Metastable fcc structures using ultrathin layers of metastable fcc Co(001) and fcc Cu(001) were grown by molecular-beam epitaxy. The growth was studied using reflection high-energy electron-diffraction (RHEED) patterns and RHEED intensity oscillations. The magnetic properties were investigated by employing ferromagnetic-resonance (FMR) and surface magneto-optic Kerr effect (SMOKE) techniques. A detailed discussion of the underlying physical mechanisms in FMR and SMOKE studies is presented. The temperature and thickness dependences of the perpendicular uniaxial and fourfold in-plane anisotropies are given and discussed. The role of lattice strains in magnetic anisotropies is demonstrated. FMR measurements revealed that the magnetic properties of single Co layers are different from those in Co/Cu/Co trilayers becuase of a lattice-strain relaxation in the multilayer samples. The exchange coupling between fcc Co(001) layers separated by a fcc Cu(001) interlayer was studied for several structures. The exchange coupling in Co structures was found to be anisotropic. Hysteresis loops were measured by means of SMOKE. Magnetic-trilayer hysteresis loops are complex. Micromagnetic calculations were carried out to explain their main features.

I. INTRODUCTION

Ultrathin magnetic metallic structures have become important in material science. Interest follows from the ability to grow epitaxially a variety of systems. fcc Co(001), a metastable structure, is stabilized at low temperatures by using a Cu(001) surface as a template.[1] Though much attention has been given to studies of the growth and electronic-state properties of this system, relatively little is known about its basic magnetic properties. This paper provides a detailed account of the magnetic properties of ultrathin layers of fcc Co(001) and the interactions between ultrathin layers of fcc Co(001) separated by the epitaxial layers of fcc Cu(001).[2]

The methods of growth, tools for characterization, and descriptions of the systems prepared are discussed in Sec. II. Reflection high-energy electron-diffraction (RHEED) patterns and RHEED intensity oscillations help to demonstrate the quality of the films produced.

Section III is devoted to the techniques for the magnetic measurements. The power of ferromagnetic resonance (FMR) in determining all the basic magnetic properties is explained. The experimental details of our Kerr-effect rotation apparatus are given. The use of the Kerr effect and interpretation of hysteresis loops for magnetic structures consisting of two ferromagnetic layers separated by a nonmagnetic interlayer (magnetic trilayer) are presented.

In Sec. IV experimental results are given for individual Co layers and for sandwiches of these layers separated by Cu. The measurements on the individual layers are used to extract the important magnetic anisotropies and contributions to the damping of the FMR. The coupled layers are used to determine the propagation of the exchange interaction across Cu and its effect on the magnetic hysteresis. The addition of a tightly coupled ultrathin layer of Fe on the far side of a Co layer is used to modify the magnetic properties of the Co layer. It will be shown that the trilayer structure which employs such a Cu/Fe layer dramatically modifies the exchange coupling through the Cu interlayer.

II. GROWTH AND STRUCTURE OF fcc Co(001)

The Cu(001) substrate preparation and growth of Co(001) have been described elsewhere.[3] A single-crystal Cu disk, 3 mm thick and 20 mm in diameter, characterized by a mosaic spread of less than 0.1°, was cut so that the [001] crystallographic orientation was within 0.2° of the (001) axis. The Cu crystal was polished using diamond paste. After insertion into the ultrahigh-vacuum (UHV) system, the crystal surface was prepared by cyclic sputtering ($V_{ion}=600$ eV, $I_{ion}=4$ μA/cm^2, 15 min) and annealing (1000 K, 10 min). The total cycling time required to obtain an uncontaminated surface with large atomic terraces was 1 week. After this treatment the surface showed sharp low-energy electron-diffraction (LEED) and RHEED patterns and no visible contamination in the Auger electron spectra. In addition, scanning tunneling microscope (STM) micrographs of the Cu(001) templates showed large extended atomic terraces (some up to 200 nm wide), separated by bands of piled-up monoatomic steps.[3]

The epitaxial growth of ultrathin fcc Co(001) films presented here was carried out in a Physical Electronics MBE-400 system. This molecular-beam epitaxy (MBE) system was equipped with RHEED, which allowed one to monitor the growth, and a double-pass cylindrical-mirror analyzer (CMA) which permitted Auger electron spectroscopy (AES) studies and x-ray photoelectron spectroscopy (XPS). A magnifying lens focused the intensity from a small area of the RHEED screen onto a photomultiplier tube in order to follow the intensity of the RHEED specular spot as a function of the film thickness during growth.

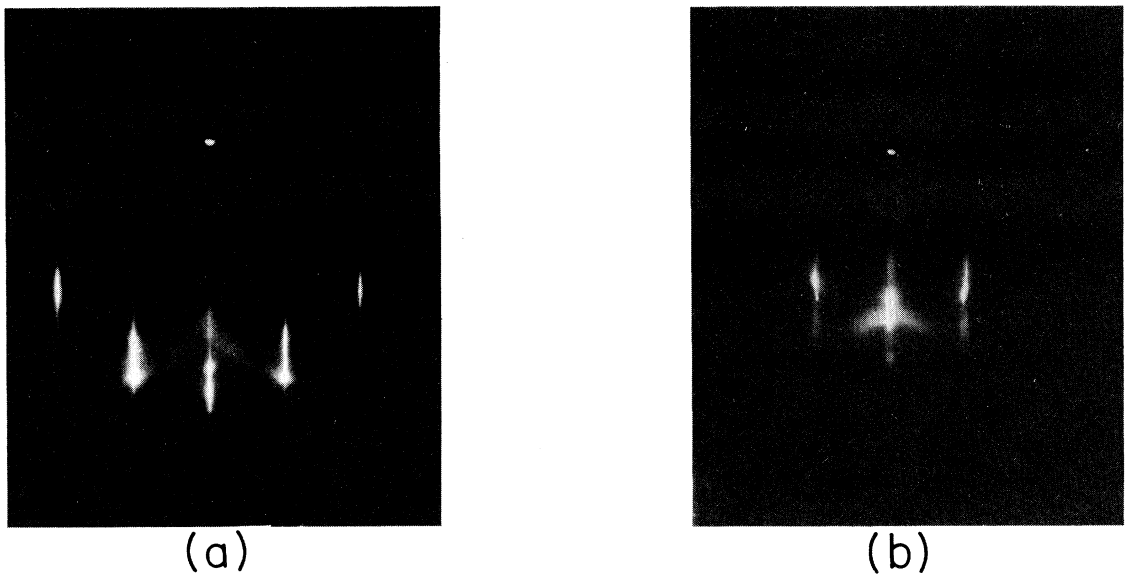

FIG. 1. RHEED patterns corresponding to {110} azimuths. (a) Cu(001); (b) 4 ML of Co(001) grown on a Cu(001) substrate.

Films were grown from clean atomic beams in a vacuum which remained in the low-10^{-10}-torr range during deposition. Beams of Cu, Co, Fe, or Au were created using a tantalum boat for Cu, a tungsten wire for Fe and Co, and a pyrolytic BN crucible for the Au depositions. The deposition rates were slow, typically ~ 1 monolayer (ML)/min. This is important when the substrate temperature is held at room temperature. Some growths were performed at higher temperatures (330–410 K) (see Tables I and IV for the details).

The quality of the growth was monitored by means of the RHEED patterns and RHEED intensity oscillations. The role of surface roughness on the amplitude of RHEED intensity oscillations was studied by means of computer simulations.[4] If three or more atomic layers grow at one time, RHEED oscillations are not sustained. In our view the presence of well-defined oscillations and sharp RHEED patterns indicates a good epitaxial growth with its surface roughness confined mainly to the top two atomic layers. Films evolving in this manner will be classified as "layer-by-layer growth."

The RHEED patterns of Co and Cu showed well-defined epitaxy (see Fig. 1). The horizontal width of the RHEED streaks determined a lower bound for an average terrace size. It was found to be 40 nm for well-prepared Cu substrates, 35 nm for Cu films grown on Co, and 20 nm for Co films grown on Cu, all room-temperature growths. The regular periodicity of the RHEED oscillations establishes the time required to form a full atomic layer. The film thickness determined from the RHEED oscillations was in very good agreement with that measured using a quartz-crystal-thickness monitor. Co layers grown on a Cu substrate acquire a regular periodicity after the second atomic layer. The outer (second) Co film grown on a Cu interlayer establishes a regular RHEED oscillation periodicity after the third atomic layer (see Fig. 2). This behavior is caused by a phase adjustment of the RHEED oscillations due to a downward funneling process that fills the voids left earlier.[5]

In a majority of our growths, either the maxima or minima of the RHEED oscillations were close to an integral number of monolayers (within 0.2 ML). That means that the RHEED oscillation phase varied by π from one sample to another. However, the RHEED oscillation phase usually remained the same within the

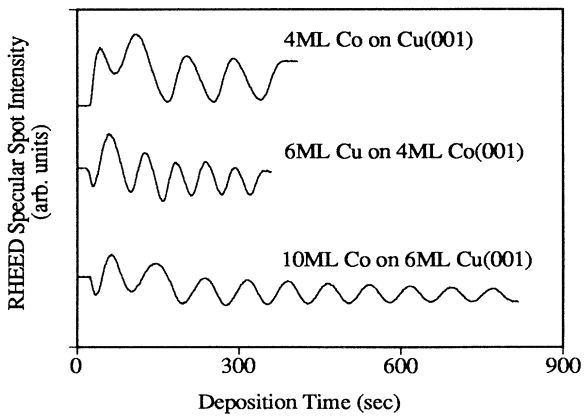

FIG. 2. RHEED intensity oscillations observed during the growth of the Cu/(Co)$_4$/(Cu)$_6$/(Co)$_{10.3}$/Cu sample. The RHEED intensity was monitored at the specular spot of the RHEED pattern. The electron beam was directed at an angle of 1° with respect to the sample surface. Note that it requires two to three atomic layers to establish regular RHEED oscillation periodicities.

given structure; that means that all growths carried out on the same substrate reached an integral number of monolayers either at a RHEED oscillation maximum or at a minimum. It appears that the RHEED oscillation phase was affected by substrate features, as yet unknown, which changed during the preparation of a new substrate.

All samples were covered by an epitaxial layer of Au before being exposed to ambient conditions. Au grows on Cu(001) substrates in the (111) orientation. There are two orientations of the Au(111) with respect to the Cu(001). These are rotated by 90° (or, equivalently, by 30°). This results in RHEED patterns characterized by an overall 12-fold in-plane azimuthal symmetry.

All of the structures were grown on the same Cu(001) crystalline disk which was re-prepared by sputtering for 2 h at 100 °C to remove the previous structure, followed by $\frac{1}{2}$-h sputtering at 400 °C, and then a flash anneal at 650 °C.

The fcc Co structure grown on Cu(001) substrates has been extensively studied by means of LEED.[6] It has been shown that at least the first 10 ML have a $p(1\times1)$ symmetry with the in-plane spacing given by that of the Cu(001) template. Our RHEED patterns support that view. Since the lattice constant in bulk fcc Co is 0.3548 nm, epitaxially grown Co(001) on Cu(001) is laterally expanded by 1.5%. LEED I-V curves[6] and thermal-energy atomic scattering[7] show evidence that there is a tetragonal distortion with the vertical spacing of the Co(001), 0.174 nm, smaller by $\sim 3\%$ than that expected for an undistorted fcc structure. The Co(001) on Cu(001) is tetragonally compressed along the surface normal. These lattice distortions significantly influence the magnetic properties of Co(001) based structures (see Sec. IV).

III. EXPERIMENTAL TECHNIQUES

Basic magnetic properties, such as the effective demagnetizing field $4\pi M_{\rm eff}$, the magnetic in- and out-of-plane anisotropies, the spectroscopic splitting factor g, and the Gilbert damping parameter G, were studied by means of the FMR technique. dc magnetization loops were investigated by means of the surface magneto-optical Kerr effect (SMOKE). The SMOKE measurements were carried out at room temperature only; the FMR studies were performed both at room and at liquid-N_2 temperatures.

A. FMR technique

The power of the FMR technique derives from the dependence of the rf susceptibility on all participating torques. The rf susceptibility can be calculated from the Landau-Lifshitz (LL) equation of motion:

$$-\frac{1}{\gamma}\frac{\partial \mathbf{M}}{\partial t}=\mathbf{M}\times\mathbf{H}_{\rm eff}\ , \tag{1}$$

where $\mathbf{M}$ and $\mathbf{H}_{\rm eff}$ include contributions from both the static and rf components, that is, $\mathbf{M}=\mathbf{M}_s+\mathbf{m}$ and $\mathbf{H}_{\rm eff}=\mathbf{H}+\mathbf{h}+\mathbf{h}_D+\mathbf{H}_k+\mathbf{h}_G$. $\mathbf{M}_s$ is the saturation magnetization, and $\mathbf{m}$ is the rf component perpendicular to $\mathbf{M}_s$. $\mathbf{H}$ is the static magnetic field which is parallel to the sample surface (parallel configuration), and $\mathbf{h}$ is the microwave rf field parallel to the sample surface and perpendicular to the dc applied field $\mathbf{H}$. $\mathbf{h}_D=-4\pi D\mathbf{m}_\perp$ is the rf demagnetizing field perpendicular to the sample surface, and $\mathbf{m}_\perp$ is the magnetization component along the normal to the specimen surface. It should be pointed out that the demagnetizing factor D in ultrathin films is dependent on the film thickness.[8] The anisotropy field $\mathbf{H}_k$ depends on the direction of the saturation magnetization with respect to the crystallographic axes.[9] The intrinsic damping is described by the Gilbert effective-damping field $\mathbf{h}_G=i(\omega/\gamma)(G/\gamma)\mathbf{m}/M_s^2$, assuming a time dependence $e^{-i\omega t}$.

The FMR absorption line is monitored by measuring the microwave amplitude reflected from a cylindrical TE_{012} cavity which contains the sample to be measured. For a FMR system, in which the microwave frequency is locked to the sample cavity, and for light loading the reflected microwave amplitude changes linearly with the absorbed microwave power in the sample. Thus the measured FMR signal is proportional to the out-of-phase microwave susceptibility χ'': $\chi=m_\parallel/h=\chi'+i\chi''$, where $m_\parallel$ is parallel to h.

The FMR measurements were carried out at 24, 36, and 73 GHz. Microwave cavities operating in the TE_{012} mode were particularly useful since the cylindrically symmetric radial rf magnetic-field pattern permitted full 360° in-plane angular FMR studies. The measured sample formed the end wall of the microwave cavity. As the applied field was rotated about the cavity axis, the component of the microwave cavity field perpendicular to the dc field did not change.

Ultrathin films of cubic materials grown along the [001] crystallographic direction exhibit in general a tetragonal symmetry. The corresponding magnetic anisotropy energies per unit volume (averaged through the film thickness) take the form

$$E_K=-\tfrac{1}{2}K_{1\parallel}^{\rm eff}(\alpha_x^4+\alpha_y^4)-\tfrac{1}{2}K_{1\perp}^{\rm eff}\alpha_z^4-K_u^{\rm eff}\alpha_z^2\ , \tag{2}$$

where α_x, α_y, and α_z are direction cosines with respect to the cubic axes.

In the parallel configuration the fourth-order uniaxial anisotropy perpendicular to the sample surface plays a negligible role in FMR.[8] However, the surface uniaxial and fourfold in-plane anisotropies do play significant roles in ultrathin films.[8,9] The overall magnetic anisotropy includes surface anisotropy terms which can be described by

$$E_s=-K_u^s\alpha_z^2-\tfrac{1}{2}K_{1\parallel}^s(\alpha_x^4+\alpha_y^4)\ . \tag{3}$$

It is important to remember that in low-frequency studies (from dc to well above microwave frequencies) the ultrathin-film magnetic moments across the film thickness are essentially parallel to one another. These locked atomic magnetic moments form a large unit which exhibits its own magnetic properties. The magnetic torques acting on a particular atomic magnetic moment in the magnetic unit are shared equally by all the magnetic moments. Consequently, the surface anisotropies divided by the film thickness d appear as effective bulklike anisotropies:[9]

$$K_{1\parallel}^{\text{eff}} = K_{1\parallel} + \frac{1}{d} K_{1\parallel}^{s} , \tag{4a}$$

$$K_{u}^{\text{eff}} = K_{u} + \frac{1}{d} K_{u}^{s} . \tag{4b}$$

The surface anisotropies include contributions from all relevant interfaces.

The linearized LL equations of motion for the parallel configuration lead to the complex rf susceptibility

$$\chi = M_s \frac{\tilde{B} - i\Gamma}{(\tilde{B} - i\Gamma)(\tilde{H} - i\Gamma) - (\omega/\gamma)^2} , \tag{5a}$$

where $\Gamma = (\omega/\gamma)(G/\gamma M_s)$,

$$\tilde{B} = H + 4\pi M_{\text{eff}} + \frac{K_{1\parallel}^{\text{eff}}}{2M_s}(3 + \cos 4\phi) \tag{5b}$$

and

$$\tilde{H} = H + \frac{2K_{1\parallel}^{\text{eff}}}{M_s} \cos 4\phi . \tag{5c}$$

G is the Gilberg damping parameter, and ϕ is the angle between the field and an in-plane cubic axis. These equations illustrate the power of FMR measurements. The in-plane angular dependence of the resonance fields H_{FMR} determines the in-plane fourfold magnetic anisotropy $K_{1\parallel}^{\text{eff}}$. The variation of H_{FMR} with microwave frequency ω permits a determination of the effective demagnetizing field

$$4\pi M_{\text{eff}} = 4\pi D M_s - \frac{2K_u^{\text{eff}}}{M_s} \tag{6}$$

and the gyromagnetic ratio $\gamma = g|e|/2mc$, where g is the spectroscopic g factor.

In ultrathin films $4\pi D$ depends on the number of atomic layers, N. It can be shown by direct summation of dipolar fields (using the procedure described in Ref. 8) that for all but the first layer $D = 1 - u/n$, where $u = 0.2338$ for an undistorted fcc structure.

The dynamic damping can be studied by the means of the FMR linewidth ΔH, which is the field separation between the extrema of the derivation of the absorption, $d\chi''/dH$. The microwave-frequency dependence of the FMR linewidth can be described in ultrathin films as

$$\Delta H = \Delta H(0) + 1.16 \frac{\omega}{\gamma} \frac{G}{\gamma M_s} , \tag{7}$$

where the frequency-dependent part arises from the intrinsic damping caused by the time-dependent part of the spin-orbit contribution to the $3d$ valence-electron energies[10] and $\Delta H(0)$ is caused by magnetic inhomogeneities incorporated into the film structure during the growth.[11] $\Delta H(0)$ is often used as a measure of the quality of epitaxially grown films.

FMR measurements are very effective for the study of the magnetic coupling between ferromagnetic layers. The theory of exchange-coupled ultrathin trilayers (two ferromagnetic layers separated by a nonmagnetic interlayer) has been extensively reviewed and used in our recent papers.[8,12,13] Here we summarize the main features which are relevant to results presented here. As pointed out above, the magnetic moments within each ferromagnetic layer precess together as a unit. The exchange interface energy per unit area can be written in the form

$$E_{\text{ex}} = -J \frac{\mathbf{M}_1 \cdot \mathbf{M}_2}{M_1 M_2} , \tag{8}$$

where J is the exchange-coupling coefficient between the layers and $\mathbf{M}_1$ and $\mathbf{M}_2$ are the saturation magnetizations in the individual films. The trilayer exhibits two microwave-resonant modes: the microwave modes of the trilayer structure correspond to a uniform precession of the magnetization within each magnetic layer, but these precessional motions are coupled. For the acoustic mode the moments in the two films precess in phase; for the optical mode the moments in the two films precess in antiphase. The character of the magnetic coupling can be determined from the relative positions of the acoustic and optical modes. In FMR the optical mode is located at a higher field than the acoustic mode for antiferromagnetic coupling and at a lower field for ferromagnetic coupling. The positions and intensities of both modes depend in a complicated way on the strength of the exchange coupling, but they can be calculated using the LL equations of motion, which include the effective fields arising from the exchange coupling.[8] One should point out that the optical mode is only observable in FMR measurements if the individual ferromagnetic layers in the absence of exchange coupling have different resonance fields.[8] The coupling to the rf driving field is very weak if the two films have identical magnetic properties.

B. Surface magneto-optical Kerr effect

We have used a simple system operating at ambient conditions. The dc magnetic field (from -8 to $+8$ kOe) is applied in the optical plane of incidence and parallel to the sample surface. A laser beam passes through a polarizer which creates an s-polarized beam which is reflected from the sample ($\theta \sim \pi/4$). The reflected laser beam passes through a crossed-polarization analyzer and is subsequently detected by means of a photodiode. The Kerr rotation in this geometry is sensitive to the magnetization component which lies in the plane of incidence. The magnetization is confined to the plane of the sample by both the strong uniaxial anisotropy and the demagnetizing field: $4\pi M_{\text{eff}} \sim 40$ kG. The longitudinal Kerr effect is proportional to the magnetization along the dc applied field. A single 1-min pass around a hysteresis loop gives a signal-to-noise ratio of ~ 20 for a 4-ML-thick Co film.

The interpretation of hysteresis loops is generally difficult. One has to minimize the total magnetic energy, which includes the magnetocrystalline, Zeeman, and exchange energies. Sample imperfections can nucleate domain walls and trigger configurational transitions. Only two extreme limits can be treated numerically in a convincing manner. In the first limit one assumes that the film is magnetically very soft and that appropriate domain-wall nucleation processes bring the film to the lowest energy available in a given applied magnetic field.

These calculations are limited to homogeneous solutions which ignore inhomogeneities such as sample imperfections. Sample imperfections are not only responsible for the domain-wall nucleation, but are also a source of domain-wall pinning, which can result in complex magnetization behaviors. In the second limit one assumes that the magnetic moments in the individual films change via a rotational mechanism only. For a dc field applied along the magnetic easy axis, coherent rotation rarely occurs. Usually, sample imperfections nucleate domain walls, and the wall motion takes over in negative internal effective fields; these fields are small compared with the internal fields that are associated with a pure rotation of the magnetization.

The trilayer hysteresis loops usually are difficult to interpret in their entirety. An interpretation is possible if there is a strong antiferromagnetic coupling which significantly surpasses the strength of the in-plane anisotropy. In that case the total energy is governed by the Zeeman and antiferromagnetic exchange energies. In high magnetic fields the Zeeman energy keeps the magnetic moments of the individual ferromagnetic layers parallel. For fields less than the saturation field $H_{\rm sat}$, the antiferromagnetic coupling starts to exert its influence and results in a decreasing trilayer magnetic moment along the field as the magnetizations rotate gradually away from their parallel configuration. A minimization of the Zeeman and exchange energies, neglecting magnetocrystalline anisotropy energies, results in the condition

$$H_{\rm sat}=-\frac{J}{M_s}\left[\frac{1}{d_1}+\frac{1}{d_2}\right], \tag{9}$$

where d_1 and d_2 are the thicknesses of the individual ferromagnetic layers.

In-plane crystalline anisotropies which are comparable to the antiferromagnetic coupling complicate the interpretation of $H_{\rm sat}$. The transition from magnetizations parallel with the applied field to magnetizations that have rotated away from the applied-field direction becomes a first-order phase transition in the presence of in-plane magnetocrystalline anisotropy. It is accompanied by a discontinuity in the magnetization. This means that the field value at which the magnetization is observed to change, $H_{\rm sat}$, becomes sensitive to the properties of inhomogeneities which can nucleate a domain structure. The field at which the transition is observed to occur may not provide a direct measure of the exchange-coupling strength J, but only a lower limit. We have observed instances for nearly equal thicknesses of the two films in which the magnetization gradually decreased as the applied field was reduced until the residual magnetization (approximately 50% of the saturation magnetization) suddenly reversed in a small negative field (see Fig. 7). This behavior was not predicted either by a minimum-energy model or by a model based upon rotation of the magnetizations. However, in our view, the measurement of $H_{\rm sat}$ still provides the best estimate of the strength of the antiferromagnetic coupling which can be obtained from a Kerr-effect measurement.

For the rotational process, the total energy can be expressed in a small-angle expansion. The critical field $H_{\rm sat}$ is found by equating to zero the first derivatives of the total energy with respect to the angles which specify the orientations of the film magnetizations. For an applied field directed along a principal crystallographic axis ($\{100\}$ or $\{110\}$), the effects of anisotropy and exchange are additive, and one obtains

$$H\pm\frac{2K_{1\parallel}^{\rm eff}}{M_s}=-\frac{J}{M_s}\left[\frac{1}{d_1}+\frac{1}{d_2}\right], \tag{10}$$

where the + and − signs correspond to the dc field along the $\{100\}$ and $\{110\}$ crystallographic axis.

The SMOKE technique applied to epitaxial trilayer samples is very useful for the study of a moderately strong antiferromagnetic coupling.[12–14] As the coupling becomes weaker or begins to be ferromagnetic, the analysis is complex and the data are hard to interpret. If either the absolute value of the antiferromagnetic coupling is lower than the in-plane anisotropies or the exchange coupling becomes ferromagnetic, there is little that can be learned about their magnitudes from SMOKE; magnetizations usually remain parallel as the external field (parallel to the easy axis) is reduced to zero. A moderately weak ferromagnetic coupling (comparable to $2K_{1\parallel}^{\rm eff}/M_s$) could be measured by applying the dc field along the hard magnetic axis in trilayers which have different in-plane anisotropies in the individual layers.

We attempted to investigate the properties of these thin cobalt films by means of Brillouin light scattering[15] (BLS), but we were unable to obtain useful signals. The data of Kerkmann *et al.*[16] indicate that the BLS signals from a cobalt film 1–2 ML thick are much weaker than the signals obtained using ultrathin bcc or fcc iron films. It is estimated from a comparison of collection times that the BLS signals from thin Fe films are approximately 100 times stronger than the signals from an equivalent thickness of Co. The reason for this difference in scattering strength is unknown; it is certainly not expected from a comparison of spin-wave amplitudes in Fe and Co.

Kerr-effect signals obtained using Co films were comparable to those obtained using bcc Fe films with a similar thickness. It can therefore be concluded that the off-diagonal elements of the magneto-optic tensor must be similar for Fe and Co. A trilayer specimen was grown in which a 3-ML-thick layer of Fe was deposited on one of the Co layers $(Cu/001)/(Co)_4/(Cu)_6/(Co)_4/(Fe)_3/(Cu)_6/(Au)_{20}$. BLS signals were observed using this specimen where the intensities were comparable to those measured using 3-ML-thick single Fe films grown on Ag(001) or Cu(001).

IV. EXPERIMENTAL RESULTS AND DISCUSSION

A. Single Co layers

FMR measurements carried out at 36 GHz revealed that single Co layers posses very strong effective perpendicular demagnetizing fields (see Table I) and large in-plane fourfold anisotropies (see Table I). The values of $4\pi M_{\rm eff}$ in ultrathin Co(001) films are significantly larger

TABLE I. Single-layer samples. All measurements carried out at 36 GHz. T_s is the temperature of the substrate during the growth of the Co layer ($g=2.155$).

		295 K			77 K		
Sample	T_s (K)	H_u[a] (kOe)	$4\pi M_{\text{eff}}$ (kOe)	$\frac{2K_{1\parallel}^{\text{eff}}}{M_s}$ (kOe)	H_u[a] (kOe)	$4\pi M_{\text{eff}}$ (kOe)	$\frac{2K_{1\parallel}^{\text{eff}}}{M_s}$ (kOe)
$(Co)_{1.7}/(Cu)_{11.5}/(Au)_{20}$	330	−15.4	30.8	−0.065	−39.0	54.4	−0.60
$(Co)_{3.3}/(Cu)_6/(Au)_{20}$	375	−25.9	42.5	−1.08	−34.7	51.3	−2.65
$(Co)_4/(Cu)_6/(Au)_{20}$	300	−25.1	41.9	−1.10	−31.3	48.1	−2.21
$(Co)_{10}/(Cu)_{10}/(Au)_{20}$	355	−17.3	34.8	−1.29	−18.8	36.3	−1.81
$(Co)_4/(Fe)_3/(Cu)_{8.5}/(Au)_{20}$	300		15.6	−0.41		15.6	−0.60

[a]Using $4\pi M_s=17.87$ kG; see Eq. (11) in the text.

than the saturation induction $4\pi M_s$. Therefore, the large perpendicular uniaxial anisotropy has its hard axis along the film normal. The in-plane fourfold anisotropy has its easy axis along the {110} crystallographic directions (see Fig. 3).

1. Magnetic anisotropies

The thickness dependence of $4\pi M_{\text{eff}}$ and $2K_{1\parallel}^{\text{eff}}/M_s$ can be fit with a constant plus a linear term in the thickness d. With a limited number of samples ($d_{\text{Cu}}=3.3$, 4, and 10 ML), it is difficult to decide whether these samples also show the $1/d$ terms which are a typical signature of surface anisotropies. Sudden deterioration of the Cu substrate precluded further choices of thickness. The available data are better represented by a term linear in d than a term linear in $1/d$. The thickness-independent parts of $4\pi M_{\text{eff}}$ and $2K_{1\parallel}^{\text{eff}}/M_s$ do not change appreciably upon cooling to liquid-N_2 temperatures. However, the terms which are linear in d show a strong temperature dependence; e.g., the term linear in d for the in-plane anisotropy field even changes its sign between liquid-N_2 temperature and room temperature.

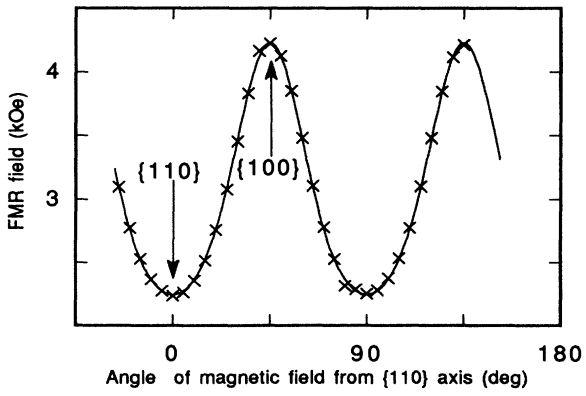

FIG. 3. In-plane angular dependence of the FMR field observed for the $(Co)_{4.3}/(Cu)_6/(Co)_4$ sample. The measurements were carried out at 36.3 GHz. The solid line represents a theoretical fit using the following magnetic properties: $4\pi M_{\text{eff}}=40.8$ kOe, $2K_{1\parallel}^{\text{eff}}/M_s=-1.05$ kOe, and $g=2.16$ (obtained from Table IV). Note that the FMR field around the easy magnetic axis changes more slowly with angle than around the hard axis. This behavior is caused by dragging the saturation magnetization behind the external field due to a strong in-plane fourfold anisotropy.

Perpendicular uniaxial anisotropies can be found from FMR by extracting $4\pi M_{\text{eff}}$ and using the formula for the finite fcc lattice:

$$H_u=\frac{2K_u^{\text{eff}}}{M_s}=4\pi\left[1-\frac{0.2338}{N}\right]M_s-4\pi M_{\text{eff}}\ , \qquad (11)$$

where N is the number of atomic layers. For fcc Co we used the saturation induction $4\pi M_s=17.87$ kG corresponding to that of hcp Co. The results of these analyses are shown in Table I.

The in-plane anisotropy decreases with an increasing sample thickness at cryogenic temperatures. The perpendicular uniaxial anisotropies decrease with an increasing film thickness at both room and liquid-N_2 temperatures. Such behavior can be expected in tetragonally distorted Co(001) films due to a relaxation of lattice strains with an increasing film thickness.[6] Phenomenologically, the thickness dependence of the perpendicular and in-plane fourfold anisotropies in Co(001) can be discussed in terms of the second- and fourth-rank tensors of magnetoelastic energy.[17] It would require a very large magnetostriction constant $\lambda=6\times10^{-4}$ to explain observed uniaxial anisotropies on bases of lattice strains of Co(001) (see Sec. II). This value is significantly larger than those observed in hcp Co and Co alloys. Therefore, the uniaxial anisotropy in Co(001) films cannot be explained by a simple magnetoelasticity theory. A large lattice relaxation would be needed,[17] ~8%, to account for the observed decrease in the in-plane anisotropy with an increasing film thickness. This value far exceeds the lattice strains as observed by LEED studies,[6] and thus again a simple linear magnetoelasticity is not suitable.

It is puzzling that the thickness dependence of the fourfold anisotropy changes its sign on heating from liquid-N_2 to room temperature. It is possible that this reversal in behavior is due to decreasing thermal fluctuations with an increasing sample thickness. However, SMOKE measurements show that even a 3-ML-thick Co film has the critical point well above room temperature, $T_c\sim600$ K.[3] The saturation magnetization in ultrathin Co films follows an Ising-type behavior, and therefore for temperatures $T\leq300$ K the thermal fluctuations should be negligible.[18] Observed reversal in the thickness depen-

TABLE II. Temperature dependence of magnetic properties for $(\underline{Co})_{1.7}/(\underline{Cu})_{11.5}/(\underline{Au})_{20}$ sample.

Temperature (K)	H_u (kOe)	$4\pi M_{\text{eff}}$ (kOe)	$\frac{2K_{1\parallel}^{\text{eff}}}{M_s}$ (kOe)
295	−15.4	30.8	−0.065
195	−28.0	43.4	−0.13
77	−39.0	54.4	−0.60

dence of the in-plane fourfold anisotropy is more likely caused by a complex dependence of the spin-orbit contribution to 3*d* valence-band energies on the sample temperature and number of atomic layers.

Recently, some controversies have occurred concerning the Curie point in a 1-ML-thick fcc Co(001) film. Beier *et al.*,[19] using spin-polarized photoemission and Kerkmann using SMOKE,[19] found the critical point T_c in 1-ML fcc Co(001) to be well above $T > 300$ K. Schneider *et al.*,[3] using SMOKE measurements, found T_c to be less than 300 K in 1-ML-thick Co. We used a somewhat thicker sample, $Cu/(Co)_{1.7}/(Cu)_{11.5}/(Au)_{20}$, than that studied in the work of Beier *et al.* and Schneider *et al.* The temperature dependence of $4\pi M_{\text{eff}}$ and $2K_{1\parallel}^{\text{eff}}/M_s$ in the 1.7-ML-thick Co film is shown in Table II.

Clearly, both $4\pi M_{\text{eff}}$ and $2K_{1\parallel}^{\text{eff}}/M_s$ are significantly decreased at room temperature when compared with thicker Co samples (see Table I). In fact, even in a dry-ice bath, the values of $4\pi M_{\text{eff}}$ and $2K_{1\parallel}^{\text{eff}}/M_s$ were still significantly lower than those observed at liquid-N_2 temperature.

FMR is not a very suitable tool to study the critical point of thin films since the large applied dc fields required partly suppress the critical fluctuations. However, the fourfold anisotropy scales as a high power law (at least fourth power) with saturation magnetization; therefore, its temperature dependence can be used to estimate the critical point T_c. Therefore, the Curie point in our 1.7-ML-thick Co is definitely not well above room temperature. In fact, the temperature dependence of $4\pi M_{\text{eff}}$ is very similar to that observed by Gradmann *et al.*[20] in the 1-ML Fe(110) on W(110).

2. *Dynamic properties*

The sample $Cu/(Co)_{10}/(Cu)_{10}/(Au)_{20}$ was extensively studied by means of FMR at 23.8, 36.3, and 72.9 GHz in order to obtain the values of $4\pi M_{\text{eff}}$ and g and the separate contributions to the linewidth using Eq. (7). The results of the analysis for $4\pi M_{\text{eff}}$ and g are shown in Table III. The value of $4\pi M_{\text{eff}}$ is weakly dependent (less than 1% variation) on the dc magnetic field (0.5–3.5–13 kOe, equivalent to the microwave frequencies 24–36–73 GHz). The g factor was found to be almost independent of field; its average value was found to be $g = 2.16$. The in-plane fourfold anisotropy $2K_{1\parallel}^{\text{eff}}/M_s$ changes, increasing by 7–8 % with an increasing dc field. The frequency dependence of the linewidth shows negligible $\Delta H(0)$, less than 5 Oe. The Gilbert-damping coefficient was found to be 3×10^8 sec^{-1}.

A zero value for $\Delta H(0)$ is unique. One expects a line broadening from the fact that the anisotropy varies with thickness. Any variation in thickness should contribute to the broadening. In the case of Fe, where the anisotropy variation with thickness changes the resonance field by 300 Oe per ML at 10 ML, the $\Delta H(0)$ was 70 Oe, which seemed to indicate very flat interfaces.[21] The variation of resonance field with Co thickness at 10 ML is 90 Oe per ML at 10 ML. This indicates that the Co surface are perhaps better.

The Gilbert-damping parameter 3×10^8 sec^{-1} is significantly larger than that observed in Fe films and bulk Fe (Refs. 21 and 22) and ($G = 0.84\times10^8$ sec^{-1}), but it is comparable to the Gilbert damping for bulk Ni (Ref. 23) (2.45×10^8 sec^{-1}). It is interesting to note that the g factors for fcc Co ($g = 2.16$) and for fcc Ni ($g = 2.19$) are also close. The deviation of the g factor from its free-electron value ($g = 2.0$) reflects the contribution of the spin-orbit coupling to the 3*d* valence-band magnetic moments. Moreover, the intrinsic damping and magnetic anisotropies in 3*d* metals also originate in the spin-orbit interaction.[10] The cubic anisotropy in bulk Ni is large at cryogenic temperatures (−2.7 kOe at liquid-N_2 temperature), and it is negative as in fcc Co layers (−2.7 kOe for 3-ML-thick Co) (see Table I). Therefore, the similar behavior of the g factors, the fourfold crystalline anisotropies, and the intrinsic Gilbert-damping parameters in fcc Co and fcc Ni suggest that the contributions of the spin-orbit interaction to their 3*d* bands are very similar.

B. Exchange coupling between Co layers

Recent measurements[24] have shown that fcc Cu interlayers can give rise to antiferromagnetic coupling between Fe and Co films. We have investigated the exchange coupling in several Co-Cu trilayer samples:

(a) $Cu/(\underline{Co})_4/(\underline{Cu})_6/(\underline{Co})_{10.3}/(Cu)_{11}/(Au)_{20}$

(b) $Cu/(\underline{Co})_4/(\underline{Cu})_6/(\underline{Co})_4/(\underline{Fe})_3/(Cu)_6/(Au)_{20}$

(c) $Cu/(\underline{Co})_{4.3}/(\underline{Cu})_6/(\underline{Co})_4/(Cu)_{17}/(Au)_{20}$

(d) $Cu/(\underline{Co})_4/(\underline{Cu})_{10}/(\underline{Co})_{10}/(Cu)_{10}/(Au)_{20}$.

TABLE III. Magnetic properties of $Cu/(\underline{Cu})_{10}/(Cu)_{10}/(Au)_{20}$ sample at different microwave frequencies.

Frequencies (GHz)	$4\pi M_{\text{eff}}$ (kOe)	$\frac{2K_{1\parallel}^{\text{eff}}}{M_s}$ (kOe)	g
24–73	34.4	−1.26 (at 24 GHz), −1.36 (at 73 GHz)	2.16
36–73	34.6	−1.29 (at 36 GHz), −1.36 (at 73 GHz)	2.16

The layers participating in the magnetic coupling are underlined, and the underlined parts (with integer numbers only) will be used to identify these specimens. SMOKE and FMR techniques were used to investigate the exchange coupling in these structures.

1. *Ferromagnetic resonance on* $(Co)_4/(Cu)_6/(Co)_{10.3}$

The magnetic properties of individual Co films give sufficiently different resonance fields (the resonance fields in 10-ML Co and 4-ML Co films were 0.32 and 0.66 kOe apart along the easy and hard axes, respectively) that FMR could be used to measure a moderately strong exchange coupling in the trilayer systems. Indeed, the sample $(Co)_4/(Cu)_6/(Co)_{10}$ exhibited optical peaks at larger fields than their acoustic counterparts, and this clearly indicated a weak antiferromagnetic coupling at both room and liquid-N_2 temperatures (see Fig. 4). It is surprising that the optical peaks were very weak in spite of the fact that they were close in field to their respective acoustic peaks. The weak optical peaks indicated that the magnetic properties of the individual Co layers changed significantly, with the result that their resonance fields were even closer than those in single layers.

Computer fits of the $(Co)_4/(Cu)_6/(Co)_{10}$ trilayer data were carried out by adjusting the values of $4\pi M_{\rm eff}$ (in each constituent layer), the in-plane anisotropy $2K_{1\parallel}^{\rm eff}/M_s$, and the exchange coupling between layers [see Figs. 4(c) and 4(d)]. Unambiguous fits were possible to achieve since the low intensity of the optical mode required the magnetic properties of the constituent layers to be very close. The position of the acoustic peak provided a good starting estimate of $4\pi M_{\rm eff}$ for the thicker Co layer. The exchange coupling was estimated from the position of the optical mode. The value of $4\pi M_{\rm eff}$ for the thinner layer was then determined from the intensity of the optical mode. Measurements along the hard and easy magnetic axes determined the in-plane crystalline anisotropy. Fits were carried out iteratively until good agreement was achieved in the resonance peak positions and in the relative intensities of the measured optical and acoustic peaks, along both the hard and easy magnetic axes. Results of our analysis are shown in Table IV.

Note that the value of $4\pi M_{\rm eff}$ obtained for the thinner Co layer was found to be substantially smaller than that obtained from measurements on a single layer. The lattice strains in the trilayer structures may well be decreased compared with strains in the single-layer structures. A relaxation of lattice strains would result in lower perpendicular uniaxial anisotropies.

It is also interesting to point out that the strength of the antiferromagnetic exchange coupling is not isotropic. It is noticeably larger along the easy axis (-0.05 ergs/cm^2) than along the hard axis (-0.028 ergs/cm^2).

2. *Ferromagnetic resonance on* $(Co)_4/(Cu)_6/(Co)_4/(Fe)_3$

We tried to increase the difference in resonance fields in the Co layers by changing the outer Co/Cu interface. The samples $Cu(001)/(\underline{Co})_4/(Au)_{20}$ and $Cu/(\underline{Co})_4/(\underline{Fe})_3/(Cu)_9/(Au)_{20}$ were grown. The first sample with the Co/Au interface showed a strange behavior. The FMR signal exhibited two separate FMR lines at 3.15 and 0.35 kOe along the easy axis and at 7.39 and 1.7 kOe along the hard axis. As shown in Sec. I, the growth of fcc Au on fcc Cu(001) templates is complex and involves two antiphase domains of Au(111). Obviously, the direct growth of Au on Co significantly alters the structure of the underlying Co film and results in two separate FMR peaks which correspond to two distinct Co phases. The two distinct Co phases are very likely caused by different lattice-strain distributions around the

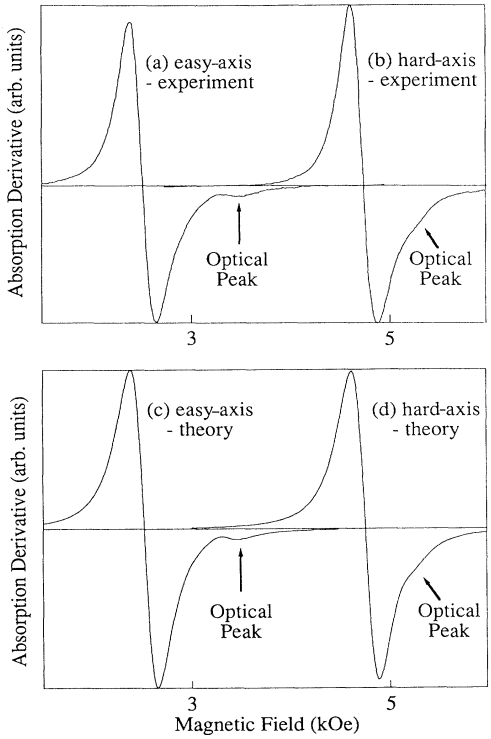

FIG. 4. FMR signal in the sample $(Co)_4/(Cu)_6/(Co)_{10.3}$ along the (a) easy and (b) hard magnetic axes at 36.3 GHz and $T=300$ K. Note that the optical peaks are weak and occur at higher fields than the acoustic peaks, and therefore the exchange coupling between the Co layers is antiferromagnetic. Note also that the optical peak along the hard axis lies closer to its acoustic counterpart than that along the easy axis. This shows that the exchange coupling is stronger along the easy axis. (c) and (d) are the calculated FMR lines using the theory of the exchange-coupled bilayers for the sample which measurements are shown in (a) and (b). The magnetic parameters for the 4 ML (A) and 10.3 ML (B) of Co(001) films were determined by fitting the positions and intensities of both the acoustic and optical peaks. The best fits were obtained by using the following parameters: $(2K_{1\parallel}^{\rm eff}/M_s)^A=-1.22$ kOe, $(2K_{1\parallel}^{\rm eff}/M_s)^B=-1.18$ kOe, $(4\pi M_{\rm eff})^A=37.3$ kOe, and $(4\pi M_{\rm eff})^B=34.2$ kOe (see Table IV). The exchange coupling along the easy axis, $J_{\rm easy}=-0.052$ ergs/cm^2, is higher than that observed for the hard axis, $J_{\rm hard}=-0.025$ ergs/cm^2.

two Au(111) antiphase domains. This specimen was unsuitable for further studies.

The second sample, $Cu/(Co)_4/(Fe)_3/Cu$, exhibited the magnetic properties of a well-behaved ferromagnetic film (see Table I). The growth of Fe shows moderately strong RHEED intensity oscillations. The Fe RHEED patterns exhibited good 90° in-plane symmetry, but the RHEED streaks along the {110} azimuths were split, indicating that the 3-ML Fe film was reconstructed.

The magnetic properties of the $Cu/(\underline{Co})_4/(\underline{Fe})_3/Cu$ film were very different from those measured for a single separate Co layer (see Table I). The presence of Fe significantly decreased $4\pi M_{\rm eff}$. In fact, $4\pi M_{\rm eff}=15.6$ kG, in the $Cu/(\underline{Co})_4/(\underline{Fe})_3/Cu$ sample, is very close to the saturation induction of fcc Co(001). Most likely, this is because the uniaxial anisotropy is significantly decreased. The in-plane fourfold anisotropy was also strongly decreased, $2K_{1\parallel}^{\rm eff}/M_s=-0.41$ kOe compared with -1.08 kOe for $Cu/(\underline{Co})_4/(\underline{Cu})_6/(Au)_{20}$. The magnetic properties of the $(Co)_4/(Fe)_3$ layer are close to an average of those observed for individual $(Co)_4$ and $(Fe)_3$ layers. This should be expected for two layers that are strongly coupled.[8]

The FMR fields in the $Cu/(\underline{Co})_4/Cu$ and $Cu/(\underline{Co})_4/(\underline{Fe})_3/Cu$ samples were very different. The resonance fields along the easy and hard axes differed by 4 and 4.6 kOe, respectively. The trilayer $(Co)_4/(Cu)_6/(Co)_4/(Fe)_3$ was well suited for the study of the magnetic coupling using the FMR technique; and indeed the optical peaks were clearly visible (see Fig. 5). Unexpectedly, the optical peaks were found at smaller fields than the acoustic peaks. The $(Co)_4$ and $(Co)_4/(Fe)_3$ layers were coupled ferromagnetically. The addition of a 3-ML Fe film on the outside of the Co layer changed the sign of the exchange coupling between the two Co layers. In contrast to the $(Co)_4/(Cu)_6/(Co)_{10}$ trilayer, the FMR measurements in this sample were very easy to

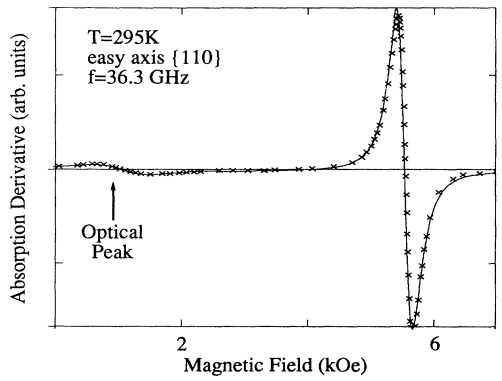

FIG. 5. FMR signal along the easy axis in the sample $(Co)_4/(Cu)_6/(Co)_4/(Fe)_3/Cu$. The solid line is a computer fit using the theory of the exchange-coupled bilayers. The parameters used to fit the data are shown in Table IV. Note that the optical peak is weak and that it occurs at a smaller field than the acoustic peak: The exchange coupling between the Co layers is therefore ferromagnetic.

TABLE IV. Magnetic properties of multilayered samples. All growths carried out at 300 K except for the $(\underline{Co})_4/(Cu)_6/(\underline{Co})_{10.3}/(Cu)_{11}/(Au)_{20}$ sample.

		295 K					77 K				
		$4\pi M_{\rm eff}$ (kOe)		$\frac{2K_{1\parallel}^{\rm eff}}{M_s}$ (kOe)			$4\pi M_{\rm eff}$ (kOe)		$\frac{2K_{1\parallel}^{\rm eff}}{M_s}$ (kOe)			
A[a]	B[b]	layer A	layer B	layer A	layer B	$J_{\rm easy}$ (ergs/cm^2)	$J_{\rm hard}$ (ergs/cm^2)	layer A	layer B	layer A	layer B	$J_{\rm easy}$ (ergs/cm^2)	$J_{\rm hard}$ (ergs/cm^2)
$(\underline{Co})_4/(Cu)_6/(\underline{Co})_{10.3}/(Cu)_{11}/(Au)_{20}$[c]		37.3	34.2	−1.22	−1.18	−0.052	−0.025	39.2	31.3	−2.01	−2.01	−0.061	[d]
$(\underline{Co})_4/(Cu)_6/(\underline{Co})_4/(\underline{Fe})_3/(Cu)_6/(Au)_{20}$		41.9	16.3	−1.10	−0.414	0.071	0.071	48.1	15.6	−2.21	−0.60	[d]	0.26
$(Co)_4/(Cu)_6/(Co)_{10.5}/(Cu)_{10.7}/(Au)_{20}$[e]			36.6		−1.27	N/A	N/A		39.7		−1.73	N/A	N/A
$(Co)_{4.5}/(Cu)_6/(Co)_4/(Cu)_{17}/(Au)_{20}$[e]			40.8		−1.05	N/A	N/A		50.9		−1.69	N/A	N/A
$(Co)_4/(Cu)_{10}/(Co)_{10}/(Cu)_{10}/(Au)_{20}$[e]			39.6		−1.00	N/A	N/A		40.1		−1.94	N/A	N/A

[a] *A* corresponds to the first ferromagnetic layer, which is $(\underline{Co})_4$ for both top samples.

[b] *B* corresponds to the second ferromagnetic layer, which is $(\underline{Co})_{10.3}$ for the first sample and $(\underline{Co})_4/(\underline{Fe})_3$ for the second one.

[c] Different growth conditions: $(Co)_4$ at 375 K, $(Cu)_6$ at 410 K, and $(Co)_{10}$ at 345 K.

[d] For samples $(Co)_4/(Cu)_6/(Co)_{10.3}/(Cu)_{11}/(Au)_{20}$ and $(Co)_4/(Cu)_6/(Co)_4/(Fe)_3/(Cu)_6/(Au)_{20}$, the optical peaks were out of the magnetic-field range at 77 K for the hard and easy axes, respectively. For these cases the computer fits were carried out for the axes which had both the optical and acoustic peaks available. The anisotropies for the $(Co)_4/(Cu)_6/(C0)_{10.3}$ trilayer were taken as an algebraic mean of the single film anisotropies from Table I. The anisotropies in $(Co)_4/(Cu)_6/(Co)_4/(Fe)_3$ multilayer were taken to be identical to those of measured single films (see Table I and text).

[e] No optical mode visible.

interpret. One did not have to change the magnetic properties of the individual layers in order to get a good fit between theory and experiment (see Tables I and IV). The exchange coupling was the only important parameter which was adjusted to fit the data obtained for fields along both the easy and hard magnetic axes (see Table IV).

In contrast with the $(Co)_4/(Cu)_6/(Co)_{10.3}$ trilayer, the metastable 4-ML Co film in the $(\underline{Co})_4/(Cu)_6/(Co)_4/(Fe)_3$ trilayer did not appear to change its magnetic anisotropies. Even the Fe lattice reconstruction did not affect the magnetic properties of the underlying Co layer. Perhaps, the $(Co)_{10.3}$ layer is responsible for the change of the $(Co)_4$ layer in the $(Co)_4/(Cu)_6/(Co)_{10.3}$ trilayer.

The ferromagnetic exchange coupling in the $(Co)_4/(Cu)_6/(Co)_4/(Fe)_3$ trilayer was found to be isotropic and to increase rapidly upon cooling. At liquid-N_2 temperatures it increased by 3.5 times; this is very close to the ratio of room and liquid-N_2 temperatures. Such a large increase in the ferromagnetic coupling with decreasing temperature was previously observed for Fe/Pd/Fe trilayers. This behavior in the Fe/Pd/Fe system was ascribed to the paramagnetic response of the Pd layer itself.[13]

Such a mechanism would be possible only if the Cu layer obtained a paramagnetic moment, through some admixture of Co. During the growth of the $(Co)_4/(Cu)_6/(Co)_4/(Fe)_3$ trilayer, the Fe lattice reconstruction might have generated structural defects which could enhance the diffusion of Co into the Cu interlayer. Paramagnetic magnetic moments on Co impurities in the Cu interlayer could then be magnetized by the exchange fields of the surrounding Co layers. In that way an induced weak magnetic moment in the Cu interlayer could provide a ferromagnetic coupling which would increase with decreasing temperature according to the Curie-Weiss law. Yet this picture is hard to reconcile with the observation that the magnetic properties of the $Ag/(\underline{Co})_4/Cu$ layer in this trilayer did not change with respect to the single layer, whereas the same layer in the $(Co)_4/(Cu)_6/(Co)_{10}$ trilayer did change its magnetic properties.

3. *Ferromagnetic resonance on $(Co)_4/(Cu)_{10}/(Co)_{10}$*

The FMR data obtained for $(Co)_4/(Cu)_{10}/(Co)_{10}$ displayed two FMR peaks (see Fig. 6). However, the low-field weak peak observed in this sample is definitely not related to the optical mode. The low-field peak in the FMR measurement occurred in the same field region where the total magnetic moment underwent a rotational process due to the antiferromagnetic coupling. This effect was recently also observed by Krebs *et al.*[25] in Fe/Cr/Fe superlattices and was argued to be due to the influence of a giant magnetoresistivity effect on the microwave absorption. The absence of the optical mode is very likely due to the fact that the resonance fields of $(Co)_4$ and $(Co)_{10}$ layers in the $(Co)_4/(Cu)_{10}/(Co)_{10}$ trilayer are very nearly equal, which results in a negligible intensity of the optical mode. This is a surprising result since the optical mode was observed in the sample $(Co)_4/(Cu)_6/(Co)_{10}$. Apparently, the magnetic properties of the individual layers are more nearly equalized in the thicker trilayer.

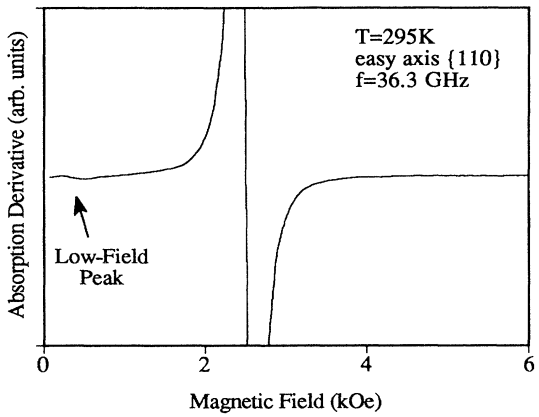

FIG. 6. FMR signal in the sample $(Co)_4/(Cu)_{10}/(Co)_{10}/(Cu)_{10}/(Au)_{20}$. The dc field is along the easy axis. The low-field weak peak is located below the saturation field, and it does not correspond to the optical mode. In order to enhance the peak in the lower field, it was necessary to increase the sensitivity of measurement, resulting in clipped higher peak.

4. *SMOKE results*

The trilayer structures $(Co)_4/(Cu)_6/(Co)_4$ and $(Co)_4/(Cu)_{10}/(Co)_{10}$ did not exhibit optical modes in the FMR measurements. In the first case the absence of an optical mode would be expected because of the similarity to the thicknesses of the Co layers. The absence in the second case may be the consequence of nearly identical magnetic properties of $(Co)_4$ and $(Co)_{10}$ in the presence of the thicker Cu layer. The exchange coupling in these trilayers could be studied only by means of the SMOKE technique.

The dc magnetic field was applied along the easy magnetic axis. The magnetization of the $(Co)_4/(Cu)_6/(Co)_4$ sample exhibited no sudden decrease as the external field was reduced: The deviation from saturation was gradual (see Fig. 7). We therefore used Eq. (10) for a rotational process to estimate the strength of the antiferromagnetic (AF) coupling. A value $H_{sat}=0.5$ kOe results in an AF coupling of $J=-0.08$ ergs/cm^2 (for $2K_{1\|}^{eff}/M_s \sim -1$ kOe).

Note also that the $(Co)_4/(Cu)_6/(Co)_4$ trilayer shows a nonzero value of the total magnetic moment at zero dc field. This remanent magnetization suggests that at zero field the magnetic moments in this trilayer are rotated by 90° with respect to each other. Clearly, the $(Co)_4/(Cu)_6/(Co)_4$ sample does not possess a simple antiferromagnetic coupling.

Micromagnetic calculations of the lowest-energy states, assumed accessible, were carried out for two layers 4.0 and 4.3 ML thick coupled by an antiferromagnetic ex-

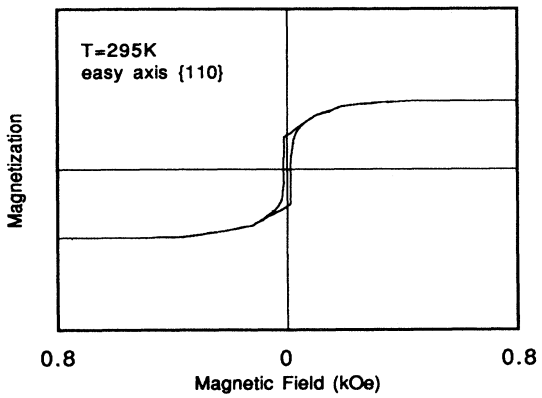

FIG. 7. SMOKE measurements of the hysteresis loop for the sample $(Co)_{4.3}/(Cu)_6/(Co)_4$. The applied field lies along the easy magnetic axis. Note that the magnetic moment in the sample deviates from saturation before zero field is reached: This indicates that the exchange coupling is antiferromagnetic. The abrupt change near zero field is due to magnetization reversal via domain walls.

change interaction. The most suitable value turned out to be $J=-0.043$ ergs/cm^2. The fourfold in-plane anisotropy was taken to be $2K_{1\|}^{\text{eff}}/M_s=-1.1$ kOe.

This coupling is similar to that observed by FMR in the sample $(Co)_4/(Cu)_6/(Co)_{10}$, $J=-0.052$ ergs/cm^2. This result is in agreement with the observations on Fe/Cu/Fe trilayers where the exchange coupling seems to depend only on the thickness of the Cu interlayer, but not on the thickness of the magnetic layers.

The numerical calculations used an algorithm which followed the free energy long paths corresponding to steepest descent.[26,27] The barrier for homogeneous rotation is sufficiently large for this model that the magnetizations would remain parallel with the external-field direction even when the field was reduced to zero. If it is assumed that the system can somehow achieve its state of lowest free energy,[27] then this model predicts a first-order phase change at an external applied-field value of 0.5 kOe with a sharp drop in the magnetization to approximately 0.3 of its saturation value. This magnetization drop corresponds to a configuration in which the layer magnetizations have rotated through angles of approximately 70°. As the field is further reduced, the magnetization directions approach a zero-field configuration in which the magnetizations are antiparallel and oriented at right angles to the field direction. This model does not describe the observed behavior (see Fig. 7).

However, the calculated variation of magnetization with applied field is similar to that observed (see Fig. 7), if one assumes an angularly dependent exchange interaction of the form

$$J=J_x+J_1[1-\cos(\theta_1-\theta_2)]\ . \tag{12}$$

If (J_x+J_1) is small, but J_1 is large, the magnetizations in zero applied field become oriented 90° from one another along two mutually perpendicular easy axes, giving a net magnetization along the applied field of $\frac{1}{2}$ the saturation value. The value $J_1=+0.02$ ergs/cm^2 is required in order that rotation away from the field direction be initiated at an applied field of 0.5 kOe.

Our studies were not primarily concerned at this point with the thickness dependence of the exchange coupling in fcc Co/Cu/Co systems on the Cu thickness. However, we carried out an additional measurement on sample (d), $(Co)_4/(Cu)_{10}/(Co)_{10}$, where the Cu interlayer was increased in thickness to 10 ML. We used this particular thickness because the bcc Fe/Cu/Fe samples exhibited a maximum in the antiferromagnetic coupling around $d_{Cu}\sim 10$ ML. The SMOKE measurement (see Fig. 8) shows clearly that sample (d) is coupled antiferromagnetically. However, its hysteresis loop exhibits a nontrivial behavior. Instead of one critical field H_{sat}, one can clearly identify two (see Fig. 8), one at ~ 0.6 kOe and the other at ~ 0.25 kOe. The presence of the second critical field is not predicted by any simple magnetization rotation mechanism. In order to explain the two extended magnetization plateaus shown in Fig. 8, it was necessary to invoke an angularly dependent exchange interaction of the form of Eq. (12). If one uses $J_x=-0.060$ ergs/cm^2, $J_1=0.015$ ergs/cm^2, along with $d_1=1.74$ nm$=10$ ML, $d_2=0.696$ nm$=4$ ML, and in-plane anisotropy fields of -1.29 and -1.10 kOe (see Table I), the minimum-free-energy model exhibits two phase transitions (see Fig. 9). The high-field transition at 0.64 kOe corresponds to a transition from a state in which the two magnetizations lie along the applied-field direction to a state in which the magnetization in the thin film lies nearly perpendicular to the field direction. The low-field transition at 0.27 kOe corresponds to the magnetization in the thin film becoming oriented antiparallel with the applied-field direction. The calculated variation of the model magnetization with field (Fig. 9) certainly resembles the data (Fig. 8), especially if the transitions were slightly smeared out because of a distribution of exchange strengths.[28] It is perhaps worth noting that, in order to produce a change in mag-

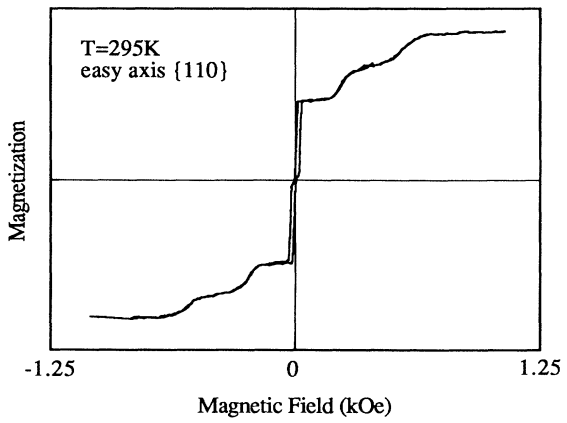

FIG. 8. SMOKE measurements of the hysteresis loop for the sample $(Co)_4/(Cu)_{10}/(Co)_{10}$. The applied field is applied along the easy magnetic axis. Relatively abrupt changes in the magnetization occur for fields of 0.6 and 0.25 kOe as well as at zero magnetic field. See detailed interpretation in the text.

netization at 0.64 kOe using the pure rotation model, it would be necessary to increase the antiferromagnetic exchange coupling to -0.127 ergs/cm^2. The resulting phase transition would cause a flip of the magnetization in the thin film from parallel to antiparallel with the applied-field direction.

One could argue that the state of lowest energy is not always achieved. The growth of nucleated domains requires that there be a negative field creating an unstable region to be swept away. A lower-energy state is then achieved in negative fields, but not necessarily in positive fields. The sample $(Co)_4/(Cu)_6/(Co)_{10}$ shows that ultrathin films can exhibit this type of behavior. The FMR data showed that the $(Co)_4/(Cu)_6/(Co)_{10}$ sample is coupled antiferromagnetically with the exchange coupling $J=-0.05$ ergs/cm^2 and yet its hysteresis loop is quite rectangular (see Fig. 10). The domain walls are nucleated in very low reversed fields and result in the magnetic-moment reversal upon crossing zero applied field. This sample does not follow the path of a minimum energy. If it did, the exchange strength $J=-0.05$ ergs/cm^2 would result in a decreasing magnetic moment for dc fields $|H|<0.6$ kOe. Clearly, the magnetization processes in ultrathin films can be very complex and the interpretation of hysteresis loops can be nontrivial.

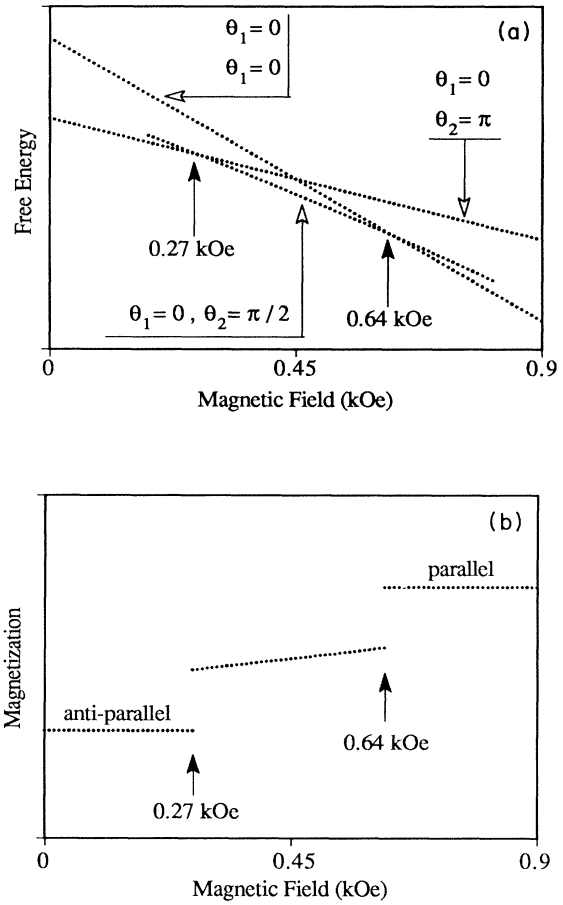

FIG. 9. (a) Magnetic-field dependence of the free energy for a model consisting of a 4-ML Co film exchange coupled with 10-ML Co film. The external field is applied along an easy magnetic axis. The parameters used in the calculation are $4\pi M_s=17.87$ kOe for each film, effective in-plane anisotropy fields $2K_{1\|}^{\text{eff}}/M_s=-1.10$ kOe (4-ML film) and $2K_{1\|}^{\text{eff}}/M_s=-1.29$ kOe (10-ML film), and an angularly dependent antiferromagnetic exchange coupling with $J_x=-0.060$ ergs/cm^2 and $J_1=0.015$ ergs/cm^2 [see Eq. (12) of the text]. The lowest free energy is obtained for a phase change at 0.64 kOe, where the magnetization in the thin film rotates into the easy-axis direction which is perpendicular to the applied-field direction, followed by a second phase change at 0.27 kOe, where the magnetization in the thin film becomes antiparallel with the magnetization in the thick film. (b) The magnetic-field dependence of the magnetization for the model of (a) assuming that the free energy can reach its minimum value at any applied field.

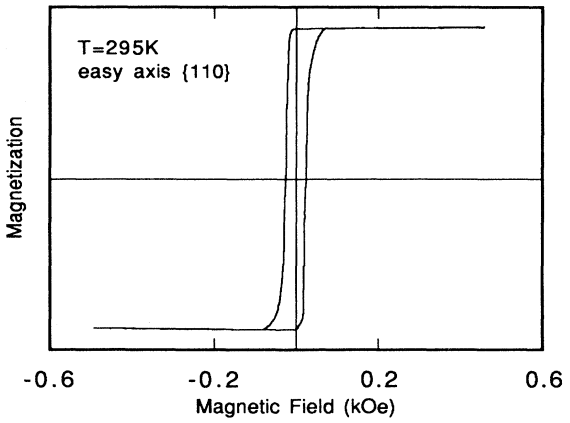

FIG. 10. SMOKE measurement of the hysteresis loop in the sample $(Co)_4/(Cu)_6/(Co)_{10}$. The applied field is along the easy magnetic axis. Co layers in this sample are coupled antiferromagnetically ($J=-0.052$) (see Table IV). Note that the hysteresis loop in this sample is square. The fourfold in-plane anisotropy $2K_{1\|}^{\text{eff}}/M_s\sim 1.2$ kOe holds the magnetic moments along the easy axis. No drop in the total magnetic moment was observed at the domain-wall nucleation field 0.5 kOe (corresponding to $J=-0.052$ ergs/cm^2); therefore, this sample does not follow the path of minimum energy.

V. SUMMARY

Ultrathin structures with one or two layers of fcc Co(001) were grown by means of MBE. RHEED patterns and RHEED intensity oscillations were used to characterize their growth. The magnetic properties of ultrathin Co(001) layers surrounded by fcc Cu(001) were investigated using the FMR technique. Trilayers of two magnetic layers separated by a nonmagnetic layer were studied using FMR and SMOKE.

It was shown that ultrathin Co(001) layers surrounded by fcc Cu(001) have a strong perpendicular uniaxial an-

isotropy with its hard axis along the film normal, resulting in a strong magnetic easy plane $4\pi M_{\text{eff}} \sim 40$ kOe. The fourfold in-plane anisotropy is also strong ($2K_{1\|}^{\text{eff}}/M_s \sim 1$ kOe) with its easy axes along the {110} crystallographic directions.

The magnetic anisotropies appear strongly dependent on the tetragonal lattice distortions of the metastable fcc Co(001) epitaxially constrained by the Cu(001) environment.

The contribution of the spin-orbit interaction to the 3*d*-band energies in strained fcc Co(001) ultrathin layers represents a major effect which cannot be explained on the basis of simple magnetoelastic terms.

The similar magnitude of the *g* factors, the fourfold in-plane anisotropies, and the intrinsic Gilbert damping in fcc ultrathin Co(001) layers and those of bulk Ni suggest that the contribution of the spin-orbit interaction to their 3*d* bands is very similar.

FMR and SMOKE studies of two Co(001) layers exchange coupled through Cu(001) interlayers were carried out for several structures. It has been shown that the magnetic properties of individual Cu/Co/Cu layers are significantly modified in exchange-coupled structures. In Cu/Co/Cu/Co/Cu structures the magnetic properties of the constituent Co layers are very similar despite differences in thicknesses. This results either in very weak or unobservable optical peaks in the FMR response.

Ultrathin fcc Co(001) layers become unstable when placed in direct contact with a Au layer. The Au layer significantly alters the underlying Co layer and results in two distinct Co phases having significantly different magnetic properties.

A single film of $(Co)_4/(Fe)_3$ exhibits properties expected from the strong coupling of a $(Co)_4$ and a $(Fe)_3$ layer. When combined into a trilayer $(Co)_4/(Cu)_6/(Co)_4/(Fe)_3$, the two magnetic layers retained their individual properties while coupling ferromagnetically across the Cu. This was in strong contrast with the behavior of a trilayer $(Co)_4/(Cu)_6/(Co)_{10}$ in which the coupling was antiferromagnetic and the two Co layers did not retain their individual properties.

Hysteresis loops measured by means of SMOKE showed complicated behaviors. Several types of micromagnetic calculations were carried out to interpret the magnetization measurements. The hysteresis loops in antiferromagnetically coupled trilayers do not follow a simple model of antiferromagnetic coupling. The absence of sudden jumps (first-order phase transitions) in the observed magnetization processes suggests that the exchange coupling in Co structures is laterally nonuniform. Some features of the observed hysteresis loops can be explained. These were used to estimate the strength of the exchange coupling. The values so determined were in good agreement with the FMR results.

FMR shows that the antiferromagnetic exchange coupling in Co/Cu/Co trilayers is anisotropic with the coupling larger along the easy magnetic axis. Hysteresis loops indicate that the antiferromagnetic coupling softens with increasing angle between the magnetizations of the two layers.

ACKNOWLEDGMENTS

The authors would like to thank the National Research Council of Canada for its financial support. The authors would like to also express their thanks to Dr. Folkerts and Dr. Purcell of Philips Research Laboratories for very valuable discussions concerning the interpretation of SMOKE measurements.

*Permanent address: Department of Physics, Free University, Berlin 33, Germany.

[1]L. Gonzales, R. Miranda, M. Salmeron, J. A. Verges, and F. Yndurain, Phys. Rev. B **24**, 3245 (1981).

[2]B. Heinrich, Z. Celinski, K. Myrtle, J. F. Cochran, M. Kowalewski, A. S. Arrott, and J. Kirschner, J. Appl. Phys. **69**, 5217 (1991).

[3]C. M. Schneider, P. Bressler, P. Schuster, J. Kirschner, J. J. Miguel, and R. Miranda, Phys. Rev. Lett. **64**, 1059 (1990).

[4]A. S. Arrott, B. Heinrich, and S. T. Purcell, *Kinetics of Ordering and Growth at Surfaces* (Plenum, New York, 1990).

[5]J. W. Evans, D. E. Sanders, P. A. Thiel, and A. E. DePristo, Phys. Rev. B **41**, 5410 (1990); B. Heinrich and A. S. Arrott, Phys. Rev. B (to be published).

[6]C. M. Schneider, J. J. Miguel, P. Schuster, R. Miranda, B. Heinrich, and J. Kirschner, *Science and Technology of Nanostructured Magnetic Materials,* edited by G. C. Hadjipanayis and G. Prinz (Plenum, New York, 1991); C. M. Schneider, thesis, Free University, Berlin, 1990 (unpublished).

[7]J. J. Miguel, A. Cebollada, J. M. Gallego, R. Miranda, C. M. Schneider, P. Schuster, and J. Kirschner, J. Magn. Magn. Mater. **93**, 1 (1991).

[8]B. Heinrich, S. T. Purcell, J. R. Dutcher, J. F. Cochran, and A. S. Arrott, Phys. Rev. B **38**, 1279 (1988).

[9]B. Heinrich, J. F. Cochran, A. S. Arrott, S. T. Purcell, K. B. Urquhart, J. R. Dutcher, and W. F. Egelhoff, Jr., Appl. Phys. A **49**, 473 (1989).

[10]J. F. Cochran and B. Heinrich, IEEE Trans. Magn. **MAG-16**, 660 (1980); V. Kambersky, Can. J. Phys. B **26**, 1366 (1976); V. Korenman and R. E. Prange, Phys. Rev. B **6**, 2769 (1972).

[11]B. Heinrich, J. F. Cochran, and R. Hasegawa, J. Appl. Phys. **54**, 3690 (1985).

[12]B. Heinrich, Z. Celinski, J. F. Cochran, W. B. Muir, J. Rudd, Q. M. Zhong, A. S. Arrott, K. Myrtle, and J. Kirschner, Phys. Rev. Lett. **64**, 673 (1990).

[13]Z. Celinski, B. Heinrich, J. F. Cochran, W. B. Muir, A. S. Arrott, and J. Kirschner, Phys. Rev. Lett. **65**, 1156 (1990).

[14]P. Grünberg, S. Demokritov, A. Fuss, M. Vohl, and J. A. Wolf, J. Appl. Phys. **69**, 4789 (1991).

[15]J. F. Cochran, J. Rudd, W. B. Muir, B. Heinrich, and Z. Celinski, Phys. Rev. B **42**, 508 (1990).

[16]D. Kerkmann, J. A. Wolf, D. Pescia, Th. Woike, and P. Grünberg, Solid State Commun. **72**, 963 (1989).

[17]B. Heinrich, Z. Celinski, J. F. Cochran, A. S. Arrott, and K.

Myrtle, Conference Proceedings of the Joint MMM+INTERMAG Meeting, Pittsburgh, 1991 [J. Appl. Phys. (to be published)].

[18]S. Bader (private communication); J. Tobochnik, Phys. Rev. B **26**, 6201 (1982).

[19]T. Beier, H. Jahrreiss, D. Pescia, T. Woike, and W. Gudat, Phys. Rev. Lett. **61**, 1875 (1988); D. Kerkmann, Appl. Phys. A **49**, 523 (1989).

[20]U. Gradmann, M. Przybylski, H. J. Elmers, and G. Liu, Appl. Phys. A **49**, 563 (1989).

[21]B. Heinrich, K. B. Urquhart, A. S. Arrott, J. F. Cochran, K. Myrtle, and S. T. Purcell, Phys. Rev. Lett. **59**, 1756 (1987).

[22]S. T. Purcell, B. Heinrich, and A. S. Arrott, J. Appl. Phys. **64**, 5337 (1988).

[23]G. Dewar, B. Heinrich, and J. F. Cochran, Can. J. Phys. **55**, 821 (1977).

[24]W. R. Bennett, W. Schwarzacher, and W. F. Egelhoff, Jr., Phys. Rev. Lett. **65**, 3169 (1990); S. S. P. Parkin, R. Bhadra, and K. P. Roche, Phys. Rev. Lett. **66**, 2152 (1991); D. H. Mosca, F. Petroff, A. Fert, P. A. Schroeder, W. P. Pratt, Jr., R. Laloee, and S. Lequien, J. Magn. Magn. Mater. (to be published); A. Cebollada, R. Miranda, C. M. Schneider, P. Schuster, and J. Kirschner, Phys. Rev. Lett. (to be published).

[25]J. J. Krebs, P. Lubitz, A. Chaiken, and G. A. Prinz, J. Appl. Phys. **69**, 4795 (1991).

[26]B. Dieny, J. P. Gavignan, and J. P. Rebouillat, Mater. Res. Soc. Symp. Proc. **151**, 35 (1989).

[27]W. Folkerts, J. Magn. Magn. Mater. (to be published).

[28]Recently biquadratic exchange, which is equivalent to our angular dependent exchange coupling, was observed in Fe/Cr/Fe systems, M. Ruthrig, R. Schafer, A. Hubert, R. Moster, J. A. Wolf, S. Demokritov, P. Grünberg, Phys. Status Solidi (to be published).

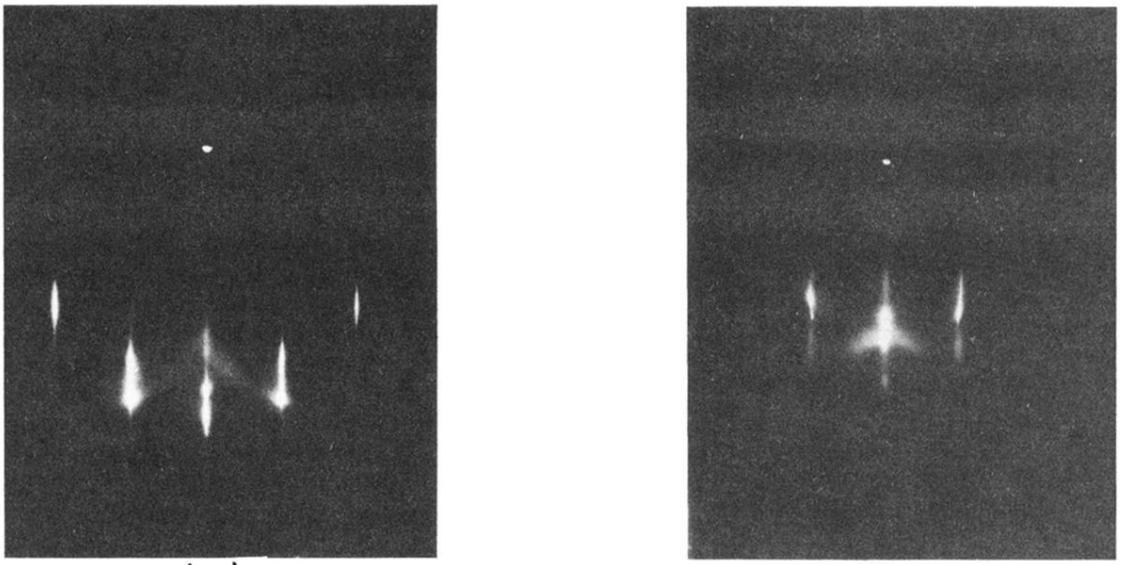

FIG. 1. RHEED patterns corresponding to {110} azimuths. (a) Cu(001); (b) 4 ML of Co(001) grown on a Cu(001) substrate.